J Mater Sci: Mater Electron (2021) 32:27744–27761

Physical, optical, and ionizing radiation shielding parameters of $Al(PO_3)_3$-doped $PbO–Bi_2O_3–B_2O_3$ glass system

Miysoon A. Alothman[1], Ateyyah M. Al-Baradi[2], Samia Ben Ahmed[3], Recep Kurtulus[4], I. O. Olarinoye[5], Taner Kavas[4], and M. S. Al-Buriahi[6,*]

[1] Department of Physics, College of Science, Princess Nourah Bint Abdulrahman University (PNU), Riyadh, Saudi Arabia
[2] Department of Physics, College of Science, Taif University, P.O. Box 11099, Taif 21944, Saudi Arabia
[3] Departement of Chemistry, College of Sciences, King Khalid University, P.O. Box 9004, Abha, Saudi Arabia
[4] Department of Materials Science and Engineering, Faculty of Engineering, Afyon Kocatepe University, Afyonkarahisar, Turkey
[5] Department of Physics, School of Physical Sciences, Federal University of Technology, Minna, Nigeria
[6] Department of Physics, Sakarya University, Sakarya, Turkey

Received: 11 July 2021
Accepted: 29 September 2021
Published online: 11 October 2021

ABSTRACT

In this report, the physical, optical, and radiation shielding features of $65PbO–(20-x)B_2O_3–15Bi_2O_3–xAlO_9P_3$ (x: 0, 2.5, 5, and 7.5 mol%) glasses coded as PBB-Al0, PBB-Al1, PBB-Al2, and PBB-Al3, respectively, are presented. Gamma-ray linear and mass attenuation coefficients were estimated via FLUKA simulations and validated by XCOM calculations for photon energies between 0.1 and 10 MeV. Also, charged particles (electron (e^-) proton (p^+), α-particle (He^{2+}) and carbon ion (C^+)) attenuation competence, Σ_R, σ_{tot}, and scattering cross-section for fast, thermal, and cold neutrons of the glasses were estimated. With an increase in AlO_9P_3 doping rate, the glass density ρ_{glass} exhibits a downward trend from 7.358 to 6.987 g·cm^{-3} for PBB-Al0 to PBB-Al3, respectively. Contrary to this, the molar volume V_m grew from 36.06 to 39.77 cm^3·mol^{-1}, as a function of insertion ratio in AlO_9P_3 from 0 to 7.5 mol%. Optical parameters such as refractive index (n), dielectric constant (ε), molar refractivity (R_m), and molar polarizability (α_m) of the glasses were found to vary depending on AlO_9P_3 content. Analysis of the obtained radiation shielding parameters revealed that gamma-ray shielding capacity of the glasses follows the trend PBB-Al0 > PBB-Al1 > PBB-Al2 > PBB-Al3. However, the influence of $Al(PO_3)_3$ on the charged particle shielding abilities of the glasses was insignificant. Furthermore, Σ_R ranged between 0.1095 and 0.11113 cm^{-1}. σ_{tot} for thermal neutron declined as the weight fraction of B, Pb, and Bi declined in the glasses. On the other hand, the scattering cross-section of cold neutrons in the glasses rose throughout the considered energy spectrum as $Al(PO_3)_3$ concentration declined in the glass matrix. Comparatively, the investigated PBB-Alx glasses are superior gamma-

Address correspondence to E-mail: mohammed.al-buriahi@ogr.sakarya.edu.tr

https://doi.org/10.1007/s10854-021-07157-x

ray photon shields than ordinary concrete, RS-360 commercial glass shield, P2 polymer, and some recently investigated glass shields. This study concludes that the presently investigated glasses have a significant role to play as alternative radiation shields in contemporary and future application of radiation.

1 Introduction

The rapid development in high-energy applications has tremendously increased particularly in the last few years. Medical interventions, food sterilization and preservation facilities, and nuclear power plants are some of the fast growing radiation application areas due to the growing world population [1–3]. Specifically, medical diagnostic and therapeutic procedures are some of the leading areas with intense use of different radiation sources [4]. Such procedures include computer tomography, brachytherapy, radiography, fluoroscopy, mammography, etc. and adopt the use of high-energy electromagnetic radiations such as X-rays and gamma-rays and energetic charged particles such as electrons and protons [5, 6]. These radiations are hazardous to humans when consistent radiation exposure occurs. This is due to the health challenges such as skin burns, cancer, cataract, or even death that may subsequently occur depending on the time of exposure and dose rate from the source [7, 8]. To mitigate against the risk of these possible harmful consequences, the use of radiation shields is essential in all technologies where these radiations are applied. Consequently, the use of different materials have been suggested as radiation shields as dictated by the type and energy of the adopted radiation, permissible dose outside the shield, volume of space available, and cost among other factors. These factors have, thus, precipitated research interest into different materials for their radiation shielding potentials within the scientific community [9, 10].

The shielding of charged particles and photons requires the use of high-density substances to attenuate the incoming rays' energy efficiently [11, 12]. With its high-density value, metallic lead and lead-based materials have become prominent [13] for this purpose. Additionally, concrete materials having relatively high densities, as well as flexibility for thickness adjustment have appeared as an alternative [14, 15]. Nevertheless, their inherently opaque appearance in visible light restricts their preferences where a transparent view is indispensable (i.e., observation window) within the radiation facilities. Accordingly, glass materials have emerged as a new perspective in radiation shielding materials and applications [16, 17], not only making use of their transparency benefits but also one can profit from wide compositional range, recycling advantages, environmental friendliness, and superior technical properties [18, 19]. Therefore, glass materials have continued to attract more attention in the last decade for potential use in radiation shielding technology.

Practically, there are a vast number of glass types and glass systems owing to the compositional flexibility. Silicates, borates, leads, germanates, tellurides, and chalcogenides are the leading ones that are commercially available in the market for different purposes. Considering that a high-density media have more effective attenuation characteristics, lead-oxide-based glass systems shine out among others [20, 21]. By the virtue of lead oxide's (PbO) high density (9.53 $g{\cdot}cm^{-3}$), an increased overall glass density value can be gained. Nonetheless, PbO alone does not have the ability for forming a glassy phase, yet other oxide contributions can aid to constitute a glassy system. Boron oxide (B_2O_3), known as a network former, is a good candidate for lead-oxide-based glass systems [22, 23]. By combining these, lead-borate (PB) glass systems can become more effective against photons and neutrons. Furthermore, another substance, bismuth oxide (Bi_2O_3), can be introduced into the PB glass network for further increment in the density because Bi_2O_3 has a density value of 8.90 $g{\cdot}cm^{-3}$ [24, 25]. With this composition, the lead-borate-bismuth (PBB) glass system is worth exploring as an alternative radiation shielding material.

The exploration of diverse materials for their radiation shielding potentials can be achieved through experimental and simulation procedures. The use of Monte Carlo codes for simulation of radiation shielding parameters of many media has become popular in contemporary times due to its fast, accurate, cheap, and safe nature. The availability

of high speed computers is another reason for the common use of this method even for materials with complex geometries and energy sources [26]. The major Monte Carlo codes commonly adopted for shielding calculations include MCNP [27], Geant4 [28], PHITS [29] EGS5 [30], PENELOPE [31], and FLUKA [32]. The FLUKA code is a multipurpose Monte Carlo tool with the capacity to simulate the transportation of more than 50 particles in diverse media structure and geometry. For the estimation of radiation shielding parameters of glasses [33], alloys [34], nanoparticles and plastic waste composites [35], Clay [36], concrete [37] etc. FLUKA has been successfully deployed with outstanding results.

This work is aimed at comprehending physical, optical, and radiation shielding features of the PBB glass system containing AlO_9P_3, which was synthesized and characterized in terms of diamagnetic aspects by [38]. For this, the glass composition of $65PbO–(20-x)B_2O_3–15Bi_2O_3–xAlO_9P_3$ (x: 0, 2.5, 5, and 7.5 mol%) was scrutinized by following physical and optical property calculations, as well as theoretical and simulation determination of the radiation shielding parameters. To the best of our knowledge, the intended glass system has not been explored for radiation shielding applications before; therefore, any findings will be of interest to those seeking alternative glass shields. Analysis of results in this report is detailed with the use of relevant tables and figures.

2 Materials and methods

The glass sysytem investigated in this study has the composition: $65PbO–(20-x)B_2O_3–15Bi_2O_3–xAlO_9P_3$ (x: 0, 2.5, 5, and 7.5 mol%). The glasses were previously synthesized and characterized by [38]. The glasses chemical definition, code, and density are presented in Table 1. The transmission of gamma-ray through a medium such as the investigated PBB-Alx follows an exponential decay according to the Beer-Lambert's law:

$$I(x) = I_o e^{-\lambda} \tag{1}$$

where I_o, $I(x)$, and λ represent the incident photon intensity, transmitted photons, and number of Mean free path (MFP) μx , respectively, for a glass of thickness x. The parameter μ is called the Linear attenuation coefficient (LAC) of the glass. μ is an important parameter that may be used to characterize the photon absorbing capacity of the glass. The knowledge of μ enables one to evaluate other relevant gamma-ray interaction particles such as Mass attenuation coefficient (MAC), Half value layer (HVL), MFP, effective atomic number Z_{eff}, and effective electron density N_{eff}, all of which are distinct parameters for characterizing photon absorption interaction in the absorbing medium. Relevant literature has discussed their relevance and how they can be calculated from the value of μ [39–41]. When μ is normalized for density i.e., $\frac{\mu}{\rho}$, the obtained parameter is called MAC. Using the Beer Lambert's equation, μ can be obtained via experimental data or Monte Carlo simulation with comparable accuracy. However, the simulation method eliminates possible exposure to radiation, is faster and cheaper, and does not require a laboratory space. In this research, μ and $\frac{\mu}{\rho}$ were obtained via FLUKA simulations and XCOM calculations. Figure 1 shows the complete simulation geometry with detailed description and procedure adopted from our published works [42]. On the other hand, the weight fraction (w_i) of the elements in the glasses was used as input parameter for the XCOM calculations. XCOM uses the mixture rule [18, 19]:

$$\left(\frac{\mu}{\rho}\right)_{\text{glass}} = \sum w_i \left(\frac{\mu}{\rho}\right)_i \tag{2}$$

where $\left(\frac{\mu}{\rho}\right)_i$ represents the $\frac{\mu}{\rho}$ for *ith* chemical constituent.

For charged particle shielding, the stopping power (S) and range are two fundamental quantities for describing the shielding ability of a material. For the investigated glass system, the S for electron, proton, α-particle, and carbon ion were evaluated for particle kinetic energies between 0.1 and 10 MeV. S describes the rate of energy loss per unit glass thickness i.e.,

$$S(E) = -dE/dx \tag{3}$$

while the projected/CSDA range is

$$R = \int_o^R dx = \int_E^0 \left(dE/dE\right) dE = \int_E^0 \frac{dE}{S(E)} \tag{4}$$

S and R (R_{CSDA} for electron) for α and C^+ was evaluated via the SRIM Monte Carlo code [43], while that of electron and proton were estimated via the use of ESTAR and PSTAR, respectively [44]. SRIM has the capacity to evaluate heavy ions' ranges and stopping powers in a material as well as simulate radiation damage in such materials. The ESTAR and PSTAR

Table 1 Sample code, chemical composition (mol%), and weight fraction (wt%) of element present in the proposed PbO–Bi_2O_3–B_2O_3–$Al(PO_3)_3$ glasses including their measured density

Glass code	Chemical composition of proposed glasses (mol%)	Chemical composition of proposed glasses (wt%)						Density (g/cm^3)
		B	O	Al	P	Pb	Bi	
PBB-Al0	$15Bi_2O_3$–65PbO–$20B_2O_3$	1.88928	11.88274	0.00000	0.00000	58.83760	27.39038	7.358
PBB-Al1	$15Bi_2O_3$–65PbO–$17.5B_2O_3$–$2.5Al(PO_3)_3$	1.61877	12.66254	0.28858	0.99382	57.61504	26.82125	7.264
PBB-Al2	$15Bi_2O_3$–65PbO–$15B_2O_3$–$5Al(PO_3)_3$	1.35928	13.41060	0.56540	1.94718	56.44226	26.27529	7.186
PBB-Al3	$15Bi_2O_3$–65PbO–$12.5B_2O_3$–$7.5Al(PO_3)_3$	1.11013	14.12881	0.83118	2.86250	55.31626	25.75111	6.987

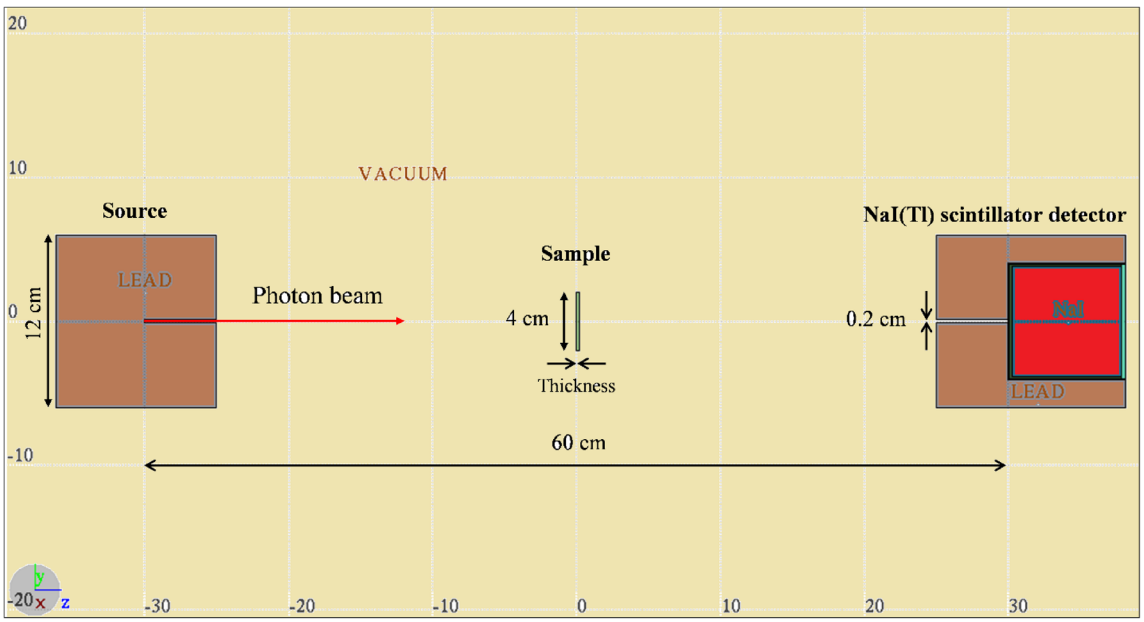

Fig. 1 Total simulation geometry

are free online computer codes which can be used to estimate the partial and total energy losses of electrons and protons of different energies, respectively, in a given material. İn all of these software, the chemical composition and density of the glasses are input parameters for the computations.

Unlike gamma radiation, the interaction of neutrons with the investigated (energy, E) glasses depends on the class of neutrons involved. Hence, different interaction cross-sections are usually used to describe the interaction of different classes of neutrons. In this study, fast, thermal, and cold neutron shielding parameters were considered. The fast neutron removal cross-section Σ_R(cm^{-1}) [45, 46], total thermal neutron cross-section σ_{tot} (cm^{-1}), and total neutron cross-section (cm^{-1}) were calculated and used to analyze the fast, thermal, and cold neutron absorption capacity of the glasses. The energy E spectrum of the cold neutron is $0.1 \leq E \leq 10$ MeV. The Σ_R and the σ_T were estimated according the additive law [45, 46]:

$$\Sigma_R = \sum w_i \left(\frac{\Sigma_R}{\rho}\right)_i \quad (5)$$

where, w_i, and $\left(\frac{\Sigma_R}{\rho}\right)_i$ is the partial density and macroscopic removal cross-section of the *ith* element

in it. $\frac{\sum_R}{\rho}$ of an element with atomic number Z are also estimated as follows:

$$\frac{\sum_R}{\rho} = 0.19Z^{(-0.743)} \quad for\ Z \leq 8; \tag{6}$$

$$\frac{\sum_R}{\rho} = 0.125Z^{(-0.565)} \quad for\ Z > 8 \tag{7}$$

$$\sigma_T = \sum_i w_i(\sigma_T)_i \tag{8}$$

3 Results and discussion

3.1 Physical property evaluations

When we mention physical properties in radiation shielding glass materials, it is generally considered to figure out the density parameter, such that the overall glass density (ρ_{glass}) is a good indication for assessing the radiation shielding competencies. This is because higher ρ_{glass} values lead to enhanced attenuation characteristics [47]. Additionally, one can simply evaluate the other essential physical parameters like molar volume (V_m), oxygen molar volume (V_O), and Oxygen packing density (OPD) by utilizing ρ_{glass} values, as well as known oxygen numbers. From this point of view, Fig. 2 shows the alterations in ρ_{glass} and V_m with the changing AlO_9P_3 content. Here, it is obvious that both parameters behave in an inverse trend to each other. With an increase in AlO_9P_3 doping rate, the ρ_{glass} exhibits a downward trend, namely from 7.358 to 6.987 g·cm^{-3} for the samples of PBB-Al0 to PBB-Al3, respectively. Contrary to this decrement, the V_m parameter is found to be in a growing trend, from 36.06 to 39.77 cm^3·mol^{-1}, as a function of insertion ratio in AlO_9P_3 from 0 to 7.5 mol%. From these findings, we may interpret that the replacement of B_2O_3 by AlO_9P_3 results in the compactness of the glass network. However, the addition of AlO_9P_3 content containing PO_4 units may translocate BO_3 or BO_4 units from B_2O_3 substance, which in turn leads to an increase in V_m values. On the other hand, the relationship between V_O and OPD value of the glasses is revealed in Fig. 3. Similar to the relationship between ρ_{glass} and V_m, the parameters, V_O and OPD, are changing inversely to each other. In detail, the order of V_O is found to be PBB-Al0 > PBB-Al1 > PBB-Al2 > PBB-Al3, whereas the OPD is calculated as 54.65, 57.49, 60.23, and 61.70 cm^{-3}·mol^{-1}

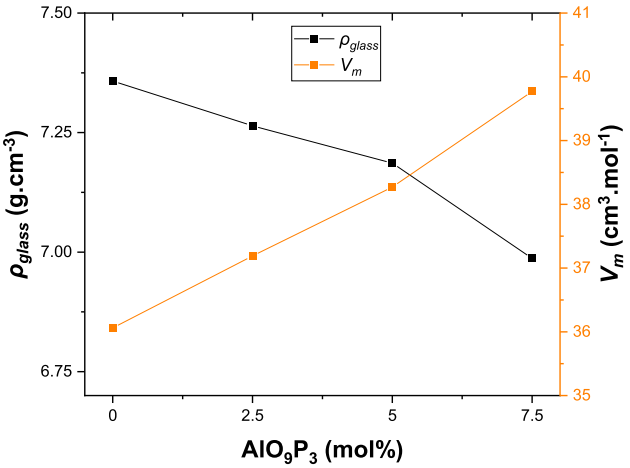

Fig. 2 The relationship between glass density (ρ_{glass}) and molar volume (V_m) with the changing AlO_9P_3 amount

for PBB-Al0 to PBB-Al3 in that respective order. These values may indicate that the number of Non-bridging oxygen (NBOs) increases as the concentration of AlO_9P_3 ascends in the glass network. In conclusion, the glass network is compacted with the contribution of AlO_9P_3, which causes a decrease in overall glass density.

3.2 Optical property determinations

The attainment of photon-matter interaction for understanding the attenuation characteristics of a glass substance is highly subjected to the determination of some significant optical parameters. In general, the enhanced optical properties aid to improve radiation shielding competencies according to the previous studies [48]. Since the authors of Ref. [38] have already measured refractive index (n), we go further with the use of the corresponding equations for figuring out selected optical parameters. In Fig. 4, one can see the variations in refractive index (n) and dielectric constant (ε) with respect to inserting AlO_9P_3 content. It is evident that both parameters are in increasing trend with the increasing doping rate. Such a situation may be associated with the compactness of the glass network which inhibits the transmitted rays throughout the glass substance. Other parameters like molar refractivity (R_m) and molar polarizability (α_m) are depicted in Fig. 5. As can be appreciated that an analogous behavior for both parameters is observable. The values for R_m are equal to 16.89, 18.81, 20.55, and 21.34, while α_m equals 6.70, 7.46, 8.15, and 8.47 for the glass series PBB-Al0

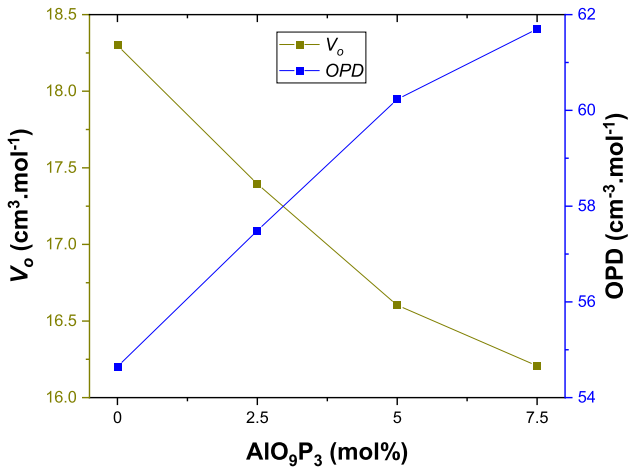

Fig. 3 The influence of AlO_9P_3 concentration on oxygen molar volume (V_O) and oxygen packing density (OPD) parameters

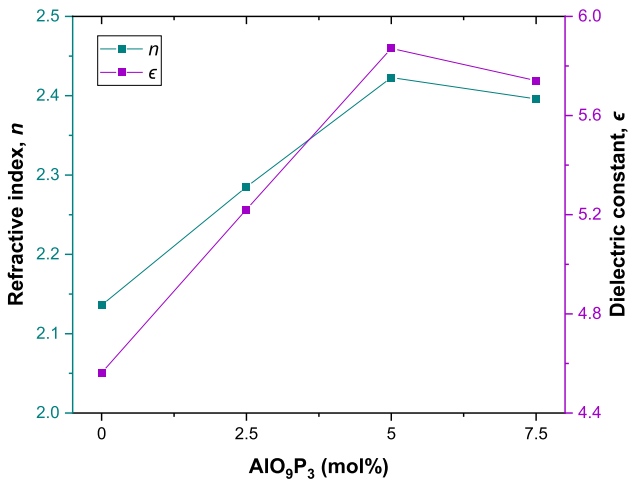

Fig. 4 The values for refractive index and dielectric constant with respect to the AlO_9P_3 contribution

to PBB-Al3. Furthermore, the refractive index-based metallization criterion (M_n) is figured out based on R_m and V_m findings, and the values are found to be 0.5317, 0.4942, 0.4630, and 0.4634 for the PBB-Al series, respectively. These values state that the glass structure displays insulator characteristics, and its insulative behavior is enhanced more as the contribution of AlO_9P_3 rises. Lastly, Fig. 6 demonstrates the changes in refraction loss (R^L) and optical transmission factor (T^{opt}) subjected to the differing AlO_9P_3 amount. Here, R^L shows a diminishing outlook, whereas T^{opt} displays an inverse behavior. This shows that the ascending insertion ratio in AlO_9P_3 gives rise to higher refraction which hinders transmitted rays. To sum up, AlO_9P_3 possesses the

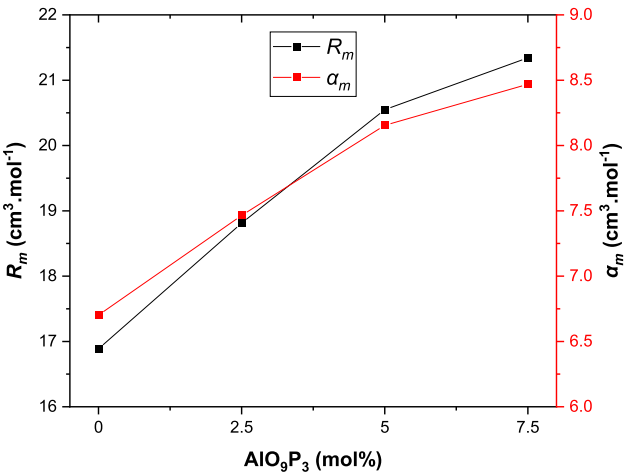

Fig. 5 The molar refractivity (R_m) and molar polarizability (α_m) of the investigated glass systems

potential for advancing the optical properties of the PBB glass system.

3.3 Radiation shielding properties

In order to ascertain the level of confidence in the FLUKA-simulated results, the values of $\frac{\mu}{\rho}$ evaluated via XCOM and FLUKA were compared quantitatively. The deviation (Dev. %) of FLUKA $\frac{\mu}{\rho}$ data from that of XCOM was estimated at all considered energies and for the four glass samples via the expression:

$$Dev.\% = \left| \frac{\left(\frac{\mu}{\rho}\right)_{XCOM} - \left(\frac{\mu}{\rho}\right)_{FLUKA}}{\left(\frac{\mu}{\rho}\right)_{XCOM}} \right| \times 100 \quad (9)$$

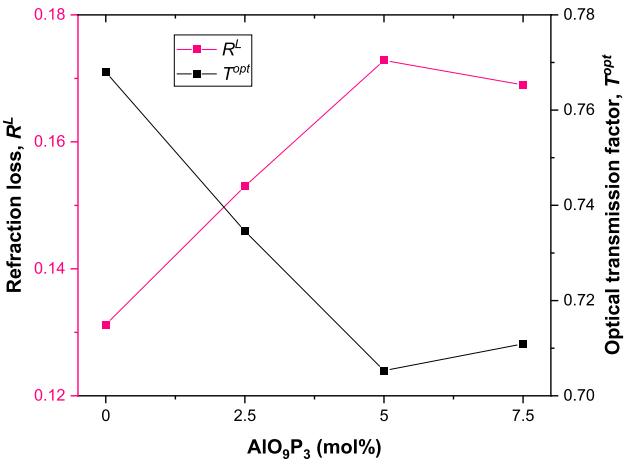

Fig. 6 The calculated refraction loss and optical transmission factors as a function of differing AlO_9P_3 content

Table 2 gives the values of $(\frac{\mu}{\rho})_{XCOM}$, $(\frac{\mu}{\rho})_{FLUKA}$, and the estimated *Dev.*% for the investigated glasses. Based on the data from the table, the deviations vary from 0.091–0.954, 0.174–0.954, 0.190–0.893, and 0.107–0.890% for PBB-Al0–PBB-Al3, respectively.

The very low deviation (< 1%) at all energies is an indication that the stimulation process is reliable and the obtained $(\frac{\mu}{\rho})_{FLUKA}$ values are concise and accurate.

The μ and $\frac{\mu}{\rho}$ are two common quantities for describing photon (X- and γ-rays) interactions within the glass system. Figure 7a and b show the changes in the value of μ and $\frac{\mu}{\rho}$ respectively as photon energy increases from 0.1 to 10 MeV. Both quantities due to their linear relationship vary in similar fashion with energy viz: maximum at the least energy, smoothly declining until it reaches minimum value at 5 MeV, and slightly increasing as energy progresses beyond 5 MeV. The corresponding maximum (minimum) value of $(\mu)_{PBB\text{-}Al0}$, $(\mu)_{PBB\text{-}Al1}$, $(\mu)_{PBB\text{-}Al2}$, and $(\mu)_{PBB\text{-}Al3}$ is 35.742 (0.30), 34.578 (0.294), 33.536 (0.289), and 31.981(0.279) cm^{-1}. The trend in the $\frac{\mu}{\rho}$ and μ values with respect to energy and glass sample can be explained in terms of the energy dependence of the different photon interaction processes and the chemical definition of the glasses.

Within the investigated energy spectrum, only three photon interaction cross-sections (σ) are significant. These are cross-sections due to photoelectric effect (σ_{PE}), Compton (incoherent) scattering (σ_{CS}), and pair production (σ_{PP}). All these are dependent on E and chemical feature (Z) of the glasses according to $\sigma_{PE} \propto E^{-3}Z^3$, $\sigma_{CS} \propto E^{-1}Z/A$, and $\sigma_{PP} \propto EZ$ [45], where Z and A is the atomic number and mass of the glass, respectively. Based on these expressions it is clear that σ_{PE} is the most significant interaction σ for $E \leq 0.6$ MeV, while σ_{cs} and σ_{PP} dominate at $0.6 < E \leq 5$ MeV and $E > 5$ MeV, respectively. Hence, the observed variation of $\mu/\frac{\mu}{\rho}$ with energy is shown in Fig. 7. Also, the expressions define the relationship between $\frac{\mu}{\rho}$ of the glasses at same energy in terms of Z (mean atomic number of the glasses).

Due to similar chemical constituents, the Z of the glasses is expected to be very close, higher for material having greater proportion of high Z constituents. This explains the strong overlapping in the curve of μ $(\frac{\mu}{\rho})$ of the glasses especially at energies beyond σ_{PE}-dominated region. The slight variation in μ was more pronounced in the low-energy region ($E \leq 0.6$ MeV) due to σ_{PE} dependence on Z^3. Although not very conspicuous, at higher energies μ and $\frac{\mu}{\rho}$ of the glasses at same energy, trend in the order: $[\mu\left(\frac{\mu}{\rho}\right)]$

Table 2 Mass attenuation coefficient of the proposed PbO–Bi_2O_3–B_2O_3–$Al(PO_3)_3$ glasses via FLUKA and XCOM at different photon energies

Energy (MeV)	PBB-Al0			PBB-Al1			PBB-Al2			PBB-Al3		
	XCOM	FLUKA	Dev.%	XCOM	FLUKA	Dev.%	XCOM	FLUKA	Dev.%	XCOM	FLUKA	Dev.%
0.1	4.85753	4.84744	0.208	4.76021	4.74917	0.232	4.66686	4.65641	0.224	4.57723	4.56765	0.209
0.15	1.77420	1.75853	0.883	1.74027	1.73250	0.446	1.70771	1.69958	0.476	1.67646	1.66931	0.426
0.2	0.88744	0.88357	0.436	0.87160	0.86901	0.298	0.85641	0.85352	0.337	0.84182	0.83962	0.261
0.3	0.36588	0.36334	0.692	0.36049	0.35814	0.653	0.35533	0.35282	0.707	0.35037	0.34795	0.690
0.4	0.21520	0.21366	0.714	0.21271	0.21116	0.726	0.21031	0.20867	0.782	0.20801	0.20644	0.754
0.5	0.15218	0.15090	0.839	0.15082	0.14956	0.832	0.14951	0.14820	0.876	0.14826	0.14711	0.776
0.6	0.11937	0.11839	0.819	0.11855	0.11754	0.854	0.11777	0.11690	0.734	0.11701	0.11618	0.708
0.8	0.08660	0.08585	0.861	0.08626	0.08558	0.784	0.08593	0.08523	0.813	0.08561	0.08494	0.791
1	0.07023	0.06970	0.755	0.07008	0.06953	0.781	0.06994	0.06942	0.740	0.06980	0.06918	0.890
1.25	0.05864	0.05808	0.954	0.05859	0.05822	0.636	0.05855	0.05830	0.428	0.05850	0.05837	0.233
1.5	0.05227	0.05192	0.668	0.05225	0.05175	0.954	0.05223	0.05177	0.893	0.05221	0.05184	0.716
2	0.04594	0.04564	0.643	0.04591	0.04570	0.444	0.04587	0.04561	0.578	0.04584	0.04589	0.107
3	0.04153	0.04132	0.505	0.04142	0.04116	0.627	0.04131	0.04114	0.408	0.04121	0.04127	0.150
5	0.04073	0.04069	0.091	0.04048	0.04012	0.892	0.04024	0.04016	0.212	0.04002	0.03985	0.430
8	0.04350	0.04340	0.240	0.04311	0.04299	0.291	0.04273	0.04258	0.352	0.04237	0.04203	0.808
10	0.04583	0.04544	0.847	0.04536	0.04529	0.174	0.04492	0.04483	0.190	0.04449	0.04410	0.859

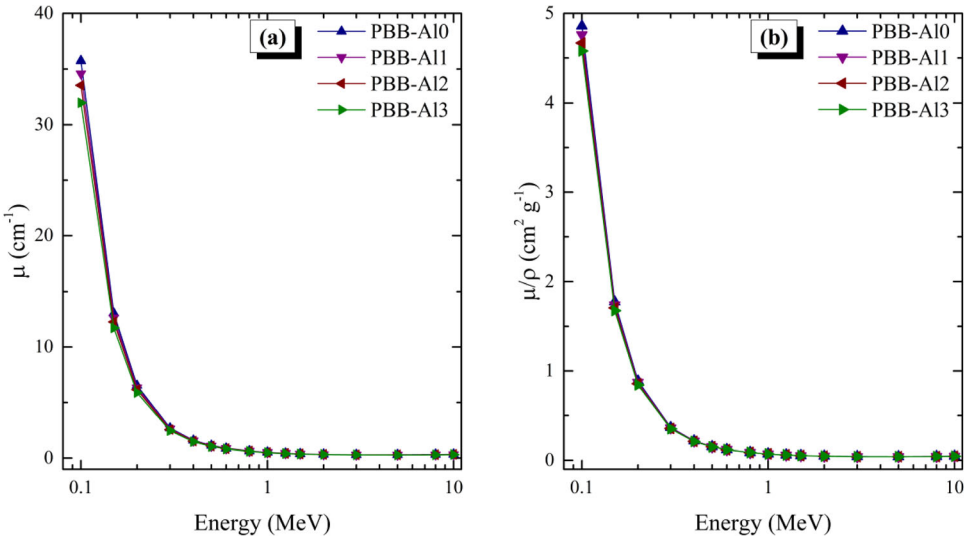

Fig. 7 Variations of **a** linear attenuation coefficient and **b** mass attenuation coefficient as a function of photon energy in the PbO–Bi_2O_3–B_2O_3–$Al(PO_3)_3$ glasses

Table 3 Fast neutron removal cross-section of elements contained in the proposed PbO–Bi_2O_3–B_2O_3–$Al(PO_3)_3$ glasses

Element	$\sum R/\rho$ (cm^2/g)	PBB-Al0			PBB-Al1		
		w_i	Partial ρ (g/cm^3)	$\sum R$ (cm^{-1})	w_i	Partial ρ (g/cm^3)	$\sum R$ (cm^{-1})
B	0.05747	0.01889	0.13901	0.00799	0.01619	0.11759	0.00676
O	0.04053	0.11883	0.87433	0.03544	0.12663	0.91981	0.03728
Al	0.02934	0.00000	0.00000	0.00000	0.00289	0.02096	0.00062
P	0.02707	0.00000	0.00000	0.00000	0.00994	0.07219	0.00195
Pb	0.01037	0.58838	4.32927	0.04488	0.57615	4.18516	0.04338
Bi	0.01030	0.27390	2.01538	0.02075	0.26821	1.94830	0.02006
Total				0.10905			0.11005
Element	$\sum R/\rho$ (cm^2/g)	PBB-Al2			PBB-Al3		
		w_i	Partial ρ (g/cm^3)	$\sum R$ (cm^{-1})	w_i	Partial ρ (g/cm^3)	$\sum R$ (cm^{-1})
B	0.05747	0.01359	0.09768	0.00561	0.01110	0.07757	0.00446
O	0.04053	0.13411	0.96369	0.03906	0.14129	0.98718	0.04001
Al	0.02934	0.00565	0.04063	0.00119	0.00831	0.05807	0.00170
P	0.02707	0.01947	0.13992	0.00379	0.02863	0.20000	0.00541
Pb	0.01037	0.56442	4.05594	0.04204	0.55316	3.86495	0.04006
Bi	0.01030	0.26275	1.88814	0.01944	0.25751	1.79923	0.01852
Total				0.11113			0.11017

$_{\text{PBB-Al0}} > [\mu\left(\frac{\mu}{\rho}\right)]_{\text{PBB-Al1}} > [\mu\left(\frac{\mu}{\rho}\right)]_{\text{PBB-Al2}} > [\mu\left(\frac{\mu}{\rho}\right)]_{\text{PBB-Al3}}$. This is consistent with the trend of the weight proportion of Pb and the mass density of the glasses. The relatively higher values of ρ, μ, and $\frac{\mu}{\rho}$ of Pb and Bi compared to the other chemical species (B, O, Al and P) in the glasses precipitated this trend.

The HVL and MFP are prominent gamma radiation interaction quantities for easily stating and comparing shielding abilities of absorbing media. While the HVL defines the required thickness for reducing the magnitude of gamma-ray dosimetric or shielding quantity by 50%, the MFP gives the mean path length between photon interaction with a particular medium. Both parameters are photon energy dependent. The shift in the value of HVL as energy and $Al(PO_3)_3$ content of the glasses changes is

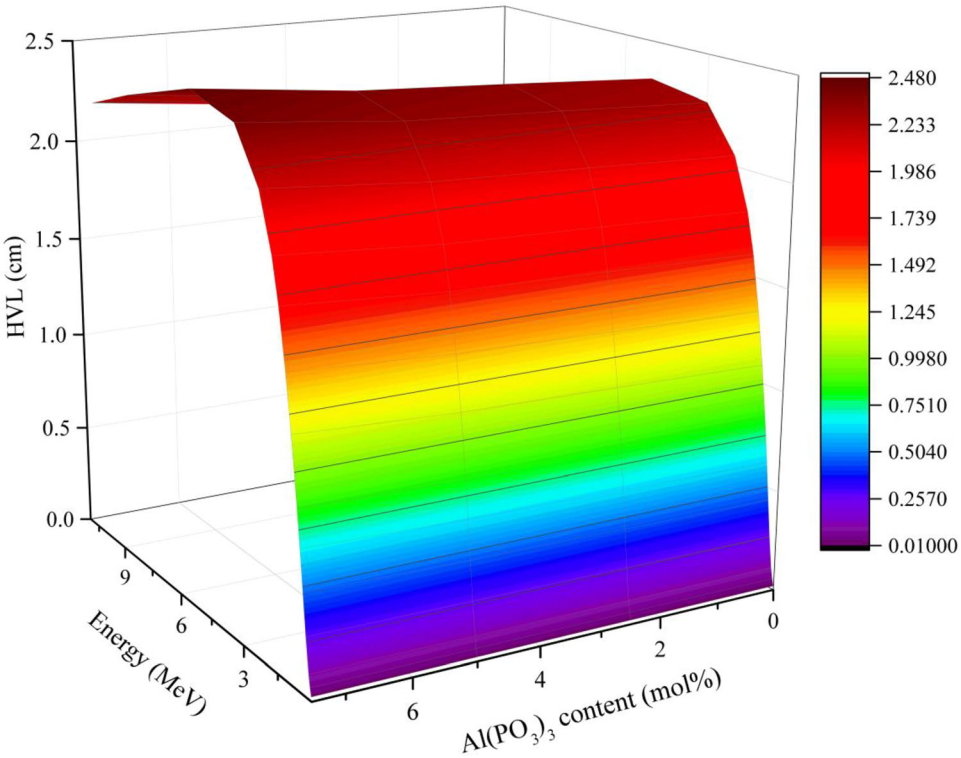

Fig. 8 Variation half-value layer as function of photon energy and $Al(PO_3)_3$ contents in the $PbO–Bi_2O_3–B_2O_3–Al(PO_3)_3$ glasses

displayed in Fig. 8. HVL grows with energy decrease up to 5 MeV due to the reductions in the values of σ_{PE} & σ_{CS}. The decline in value for E > MeV is consistent with higher value of σ_{PP}. The least HVL (0.0194 cm) was obtained for PBB-Al0 at 0.10 MeV, while the maximum is 2.479 cm at 5 MeV, an indication of decreasing photon shielding efficiency as $Al(PO_3)_3$ increases from 0 to 7.5 mol %. Similar to μ, and $\frac{\mu}{\rho}$ the differences in HVL of the glasses are less significant at energies beyond the σ_{PE}-dominated region. The photon shielding ability of the present glasses compared to other recently investigated and conventional shields was analyzed based on their relative MFP. Figure 9 displays the MFP spectra of the PBB-AL glasses in contrast to those of ordinary concrete [49], RS-360 commercial glass shield [50], P_2 polymer [51], and recently investigated BBSN5-7 [52], SBC-B35 [53], SLG6-E5 [54], and LB24 [55] glasses. The spectra show that the MFP of PBB-Al0–PBB-Al3 were all lower than those of the compared materials; an indication of superior shielding capacity. This suggests that the presently investigated glasses can effectively shield photons better than those materials; hence they are potential candidates for radiation protection in different nuclear facilities where gamma radiation is deployed and shielding required.

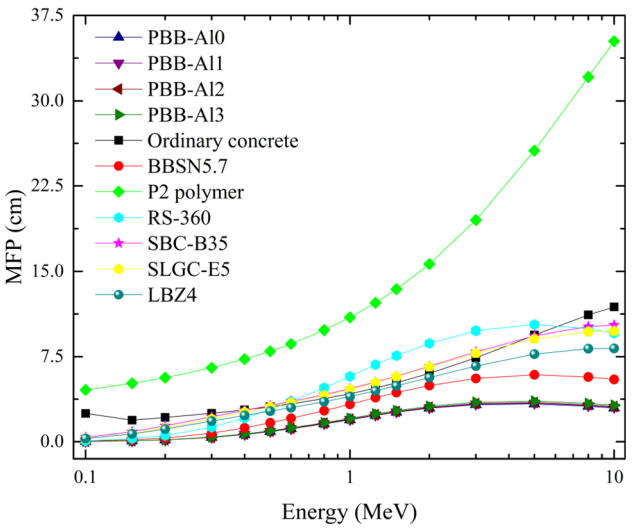

Fig. 9 Variation of mean free path as a function of photon energy for the $PbO–Bi_2O_3–B_2O_3–Al(PO_3)_3$ glasses in comparison to ordinary concrete [49], commercial RS-360 [50], P2 polymer [51], BBSN5.7 [52], SBC-B35 [53], SLGC-E5 [54], and LBZ4 [55] glasses

Figure 9 also shows that the present glasses are positioned at the top of gamma-ray shields.

The effective atomic number Z_{eff} and the effective electron density N_{eff} are important photon interaction parameters which could be analyze the shielding

Table 4 Coherent scattering cross-section (σ_{coh}), incoherent scattering cross-section (σ_{inc}), absorption cross-section (σ_{abs}), and total cross-section (σ_{tot}) of the proposed PbO–Bi_2O_3–B_2O_3–$Al(PO_3)_3$ glasses for thermal neutrons attenuation

Prepared glasses	Thermal neutron cross-section (cm^{-1})			
	σ_{coh}	σ_{inc}	σ_{abs}	σ_{tot}
PBB-Al0	1.76727	0.19763	89.14509	91.10999
PBB-Al1	1.72261	0.16027	72.26846	74.15134
PBB-Al2	1.68480	0.12808	57.72873	59.54161
PBB-Al3	1.62142	0.09816	44.21408	45.93366

ability of a medium. They relate the chemical definition of a glass with its photon shielding ability. Both parameters are proportional to energy as indicated in Fig. 10a and b. obviously, the energy dependence of Z_{eff} and N_{eff} are similar due to the relationship between them. Z_{eff} and N_{eff} decreases with photon energy between 0.1 and 1.5 MeV. Subsequently, they gradually increase with energy up to the end of the considered energy spectrum. The behavior of these quantities is in agreement with the behavior of the partial photon interaction σ with respect to energy and the atomic number of the absorbing glass. High σ_{PE} and its dependence on Z and E explains the high but rapidly declining value of Z_{eff} and N_{eff} in the σ_{PE} dominated energy. While the rise in values of the two quantities is due to the rise in σ_{PP} as energy increases. It is worthy of note that the trend: $(Z_{eff})_{PBB\text{-}Al3} < (Z_{eff})_{PBB\text{-}Al2} < (Z_{eff})_{PBB\text{-}Al1} < (Z_{eff})_{PBB\text{-}Al0}$ is consistent at all the investigated photon energies. The value of Z_{eff} varies from: 34.84–78.88, 33.54–78.55, 32.37–78.23 and 31.33–77.91 as $Al(PO_3)_3$ increases in the glasses. The slightly decreasing trend in Z_{eff} value as $Al(PO_3)_3$ content of the glasses increases can be attributed to the resulting decrease in the weight fractions of Pb and Bi (Table 1). Higher Z_{eff} is associated with a material with higher concentrations or weight fractions of higher Z elements. On the contrary, the trend of Z_{eff} is the reverse of that of N_{eff} at all energies. This is due to the direct relationship between N_{eff} and $<Z/A>$ $<Z/A>$ of the glasses; a quantity that decreases with Z_{eff} of a material. Furthermore, the range of $<Z/A>$ for many materials varies between 0.4 and 0.5, hence the narrow differences between the N_{eff} of the glasses under investigation. This narrow margin is more prominent in the σ_{CS} dominated energies as a result of σ_{CS} and its $<Z/A>$ dependence.

In gamma radiation dosimetry and shielding, the absorbed photon energy is an essential quantity for describing the photon absorption process. To quantify the absorbed energy, the mass energy-absorption coefficient $(\frac{\mu_{en}}{\rho})$ may be used. The $\frac{\mu_{en}}{\rho}$ is directly proportional to $\frac{\mu}{\rho}$ and measures the energy of γ-rays absorbed excluding secondary photons that escape the absorbing medium. Using the mixture rule similar to $\frac{\mu}{\rho}$, $\frac{\mu_{en}}{\rho}$ of the glasses $\left(\frac{\mu_{en}}{\rho}\right)_g$ was estimated from the following:

$$\left(\frac{\mu_{en}}{\rho}\right)_g = \sum w_i \left(\frac{\mu_{en}}{\rho}\right)_i \quad (10)$$

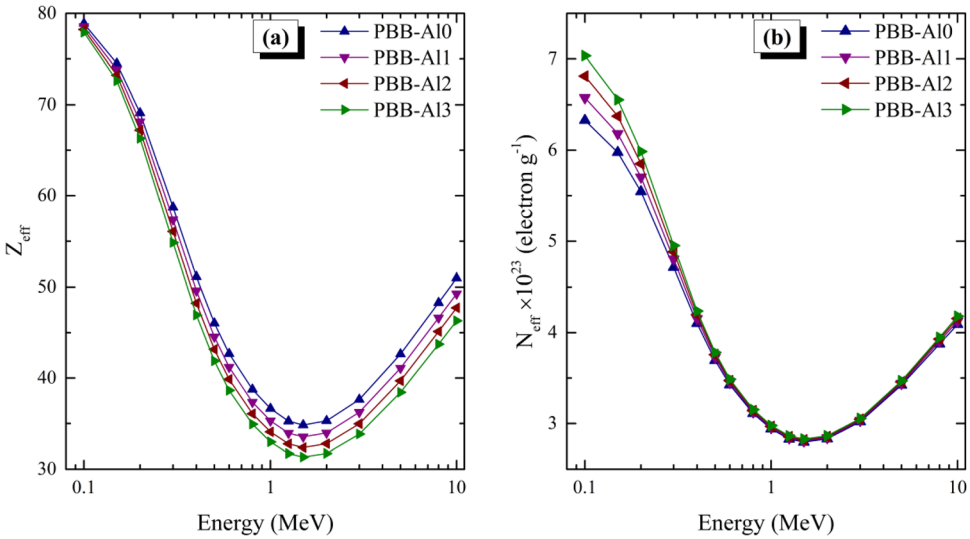

Fig. 10 Variations of **a** effective atomic number and **b** effective electron density as a function of photon energy in the PbO–Bi_2O_3–B_2O_3–$Al(PO_3)_3$ glasses

where w_i and $\left(\frac{\mu_{en}}{\rho}\right)_i$ represent weight fraction and $\frac{\mu_{en}}{\rho}$ for element i in the glasses. The energy variation of $\left(\frac{\mu_{en}}{\rho}\right)_g$ for the present glasses is shown in Fig. 11a. The energy dependence of $\frac{\mu_{en}}{\rho}$ as expected is directly proportional to that of $\frac{\mu}{\rho}$. Higher photon absorption $\frac{\mu_{en}}{\rho}$ is recorded for glasses with lower $Al(PO_3)_3$ content due to higher density and Z_{eff} in the σ_{PE}-dominated energies. Beyond this region, $\frac{\mu_{en}}{\rho}$ was almost equal for all the glasses due to the dominance of σ_{CS} and its dependence on N_{eff}.

Similarly, the gamma-ray dose constant (Γ) of the glasses (Fig. 11b) initially decrease with energy due to the significant influence of $\frac{\mu_{en}}{\rho}$ in the low-energy (σ_{PE} dominated) region of the spectrum. As energy increases, photon becomes highly penetrating and causes more ionization, hence the increasing trend of Γ as photon energy grows beyond MeV. Γ for the glasses beyond the low-energy region was almost constant irrespective of $Al(PO_3)_3$ content.

The dose rate (D) within glass thickness of 1, 5, 10, and 15 mm of PBB-Al0 – PBB-Al3 as photon energy changes is shown in Fig. 12. The strong influence of Γ on D is clear as both vary similarly with photon energy. Due to higher photon absorption within thicker glasses, D decreases as glass thickness increases at equal energy and for the same glass sample. The lowest dose rate at the different glass thickness was at 1 MeV due to the significance of Compton scattering (low absorption) of photons at this energy. Comparing D for the investigated glasses reveals that the trend is consistent with $\frac{\mu_{en}}{\rho}$ and Γ at the same energy.

Charged particle interactions are used for material characterization; hence charged particle stopping power (S_p) and range (R) are important parameters in such applications. The energy variation of total S_p (TSP) of electron (e^-), proton (p^+), α-particle (He^{2+}), and carbon ion (C^+) is depicted in Fig. 13 for the investigated PBB-Al glasses. Generally, TSP depends on E in different ways depending on the charged particle and glass medium of interest. For the present glasses, TSP for electron $(TSP)_e$ does not appear to have any significant differences; hence electron absorption in the glasses is almost equal at equal energy. However, $(TSP)_e$ initially decreases with E due to the dominance of Coulomb loses. Beyond 1.25 MeV $(TSP)_e$ grows with particle kinetic energy (T) due to the significance of radiative losses of the electron as energy increases.

For p^+, the influence of the glass density becomes clearer as the differences in $(TSP)_p$ follows the order PBB-Al3 > PBB-Al2 > PBB-Al1 > PBB-Al0 for most parts of the energy spectrum (0.1–10 MeV). Also, the interaction of p^+ in the glasses within T range is such that $(TSP)_p$ steadily decreases with respect to T due to Coulomb collisions. The behavior of He^{2+} and C^+ TSP with energy is similar, initially increasing and subsequently decreasing beyond T > 1.25 MeV. The trend of $(TSP)_{p+}$ of the glasses is sustained in those of He^{2+} and C^+. The influence of density on TSP becomes more obvious at higher energy as the quantity of charges of the particle increases. The projected range of a charged particle is the distance

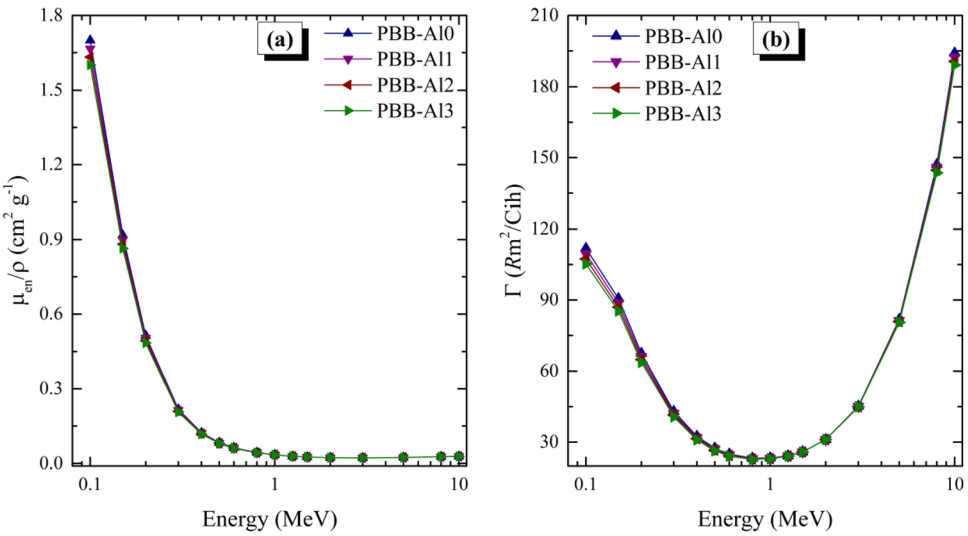

Fig. 11 Variations of **a** mass energy-absorption coefficient and **b** specific gamma-ray constant as a function of photon energy in the PbO–Bi_2O_3–B_2O_3–$Al(PO_3)_3$ glasses

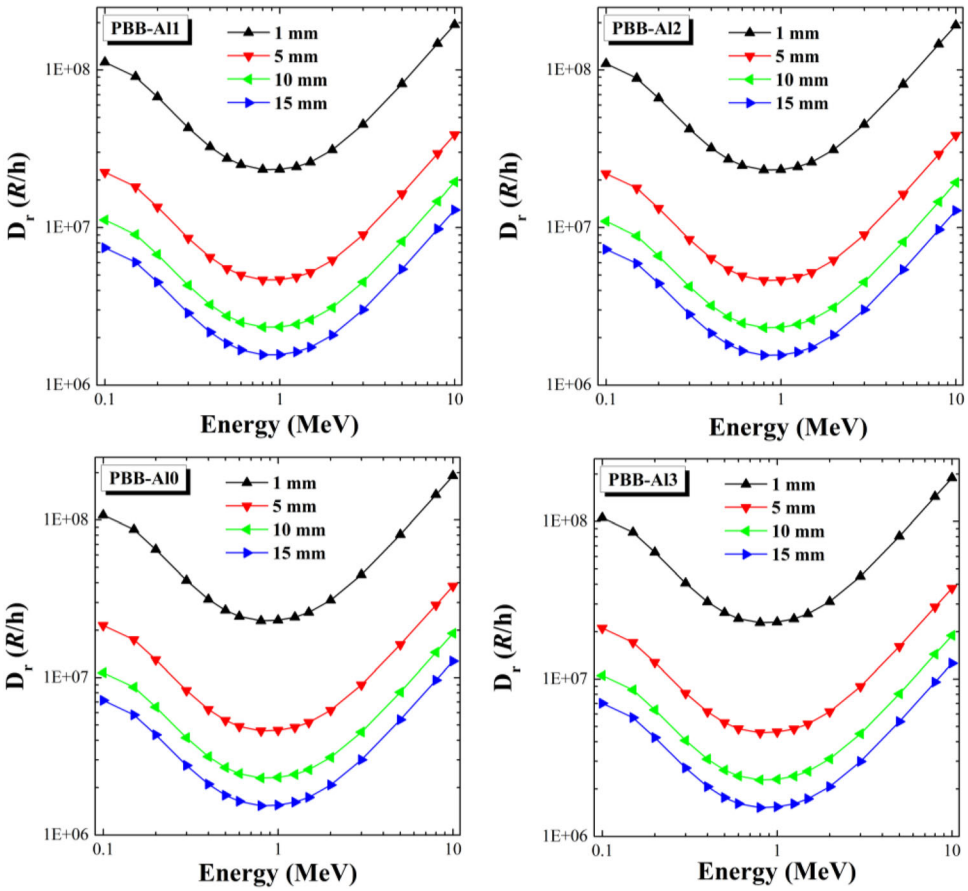

Fig. 12 Variation of gamma dose rate at different energy levels for the $PbO–Bi_2O_3–B_2O_3–Al(PO_3)_3$ glasses

moved by the particle before losing its entire energy and subsequently coming to rest. For electrons the continuous slowing down approximation is used according to Eq. 4, while for other charged particles, the projected range is calculated. Due to its charge, a particle undergoes a lot of Coulomb interactions where a fraction of its energy is lost in each interaction process. This gradual loss is called the Continuous slowing down approximation (CSDA). The total distance moved in this friction-like movement is called the CSDA range. On the other hand, the projected range is the expectation value of the mean distance moved by many of such particles. Both parameters are similar for all practical intent. According to Fig. 14, the estimated R of the charged particles (e^-, p^+, He^{2+} and C^+) and their variation with energy are similar; increasing as T grows. Higher T-charged particles penetrate through an absorber deeper. A quantitative comparison of R of all the particles of the glasses shows that for a particular particle, R is almost equal for all the glasses. Hence, the influence of $Al(PO_3)_3$ on the charged particle absorption capacity of the PB-Al glasses is not so significant.

Figure 15 displays calculated value Σ_R for the glasses. The calculation method can be understood from Table 3. İn order of increasing $Al(PO_3)_3$, Σ_R was obtained as 0.1095, 0.11005, 0.11113, and 0.11017 cm^{-1}. These values follow an off-trend pattern with respect to $Al(PO_3)_3$ content such that PBB-Al2 possesses the highest fast neutron moderating capacity. This suggests that PBB-Al2 has the optimum chemical combination of PBB-AlX glasses for fast neutron removal. Since high Σ_R are desirable for fast neutron shielding, the Σ_R value for PBB-Al2 compared to that of ordinary concrete (0.0957 cm^{-1}) [49] showed that PBB-Al2 is a better fast neutron removal ability.

The total cross-section for thermal neutrons σ_{tot} is the sum of the scattering (σ_{sc}) and absorption (σ_a) cross-sections of thermal neutrons within a medium. İt can be used to characterize the probability of thermal neutron interactions leading to absorption within the medium. The σ_{tot} of the PBB-Alx glasses are presented in Fig. 16. Obviously, the σ_{tot} declines

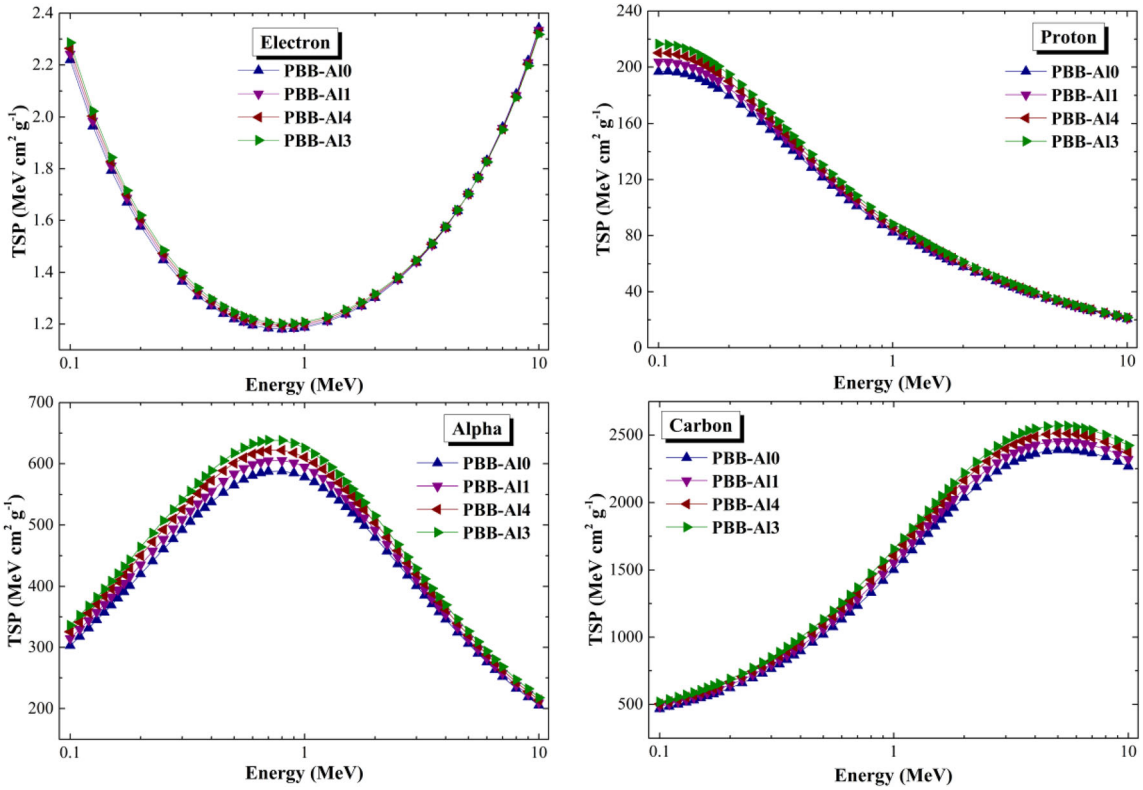

Fig. 13 Variation of total mass stopping power as a function of kinetic energy in the PbO–Bi_2O_3–B_2O_3–$Al(PO_3)_3$ glasses shown for electron, proton, alpha particles, and heavy carbon ion

in value as $Al(PO_3)_3$ increases within the glass matrix. The total cross-section for thermal neutrons varies within the range 45.9337–91.1100 cm^{-1} as $Al(PO_3)_3$ increases from 0 to 7.5 mol %. The drastic decline in the σ_{tot} is strongly related to the consequent decay in the weight fractions of B, Pb, and Bi (Table 4) as $Al(PO_3)_3$ concentration grows in the glasses. Among the chemical species in the glass matrix, B has the highest σ_a , while Pb and Bi have comparable but higher σ_{sc} compared to the other elements; hence, there is a decline observed in the value of σ_{tot} as the weight fractions of these elements drop.

Furthermore, the total scattering cross-section spectrum for neutron energies between 0.01 and 10 meV and that of their penetration depths in the glasses is depicted in Fig. 17a and b, respectively. Due to higher density and weight fractions of Pb and Bi, scattering probability follows the trend of decreasing $Al(PO_3)_3$ content at all energies. Higher scattering of neutrons correspondingly leads to lower penetration due to energy losses and , thus, the neutron penetration in PBB-Al3 < PBB-Al2 < PBB-Al1 < PBB-Al0 (Fig. 17b).

4 Conclusion

This study reports the physical, optical, and radiation shielding parameters of PBB-AlX glasses with the chemical definition $65PbO–(20–x)B_2O_3–15Bi_2O_3–xAlO_9P_3$ (x: 0, 2.5, 5, and 7.5 mol%) and coded as PBB-Al0, PBB-Al1, PBB-Al2, and PBB-Al3, respectively. Gamma-ray and charged particles (electron (e^-) proton (p^+), α-particle (He^{2+}) and carbon ion (C^+)) attenuation parameters were evaluated for energies within 0.1–10 MeV. Also, Σ_R, σ_{tot}, and scattering cross-sections for fast, thermal, and cold neutrons of the glasses were estimated. With an increase in AlO_9P_3 doping rate, the glass density ρ_{glass} exhibits a downward trend from 7.358 to 6.987 $g.cm^{-3}$ for PBB-Al0 to PBB-Al3 respectively. Contrary to this, the molar volume V_m grew from 36.06 to 39.77 $cm^3.mol^{-1}$, as a function of insertion ratio in AlO_9P_3 from 0 to 7.5 mol%. Optical parameters such as refractive index (n), dielectric constant (ε), molar refractivity (R_m), and molar polarizability (α_m) of the glasses were found to vary depending on AlO_9P_3 content. Analysis of the obtained parameters revealed that gamma-ray

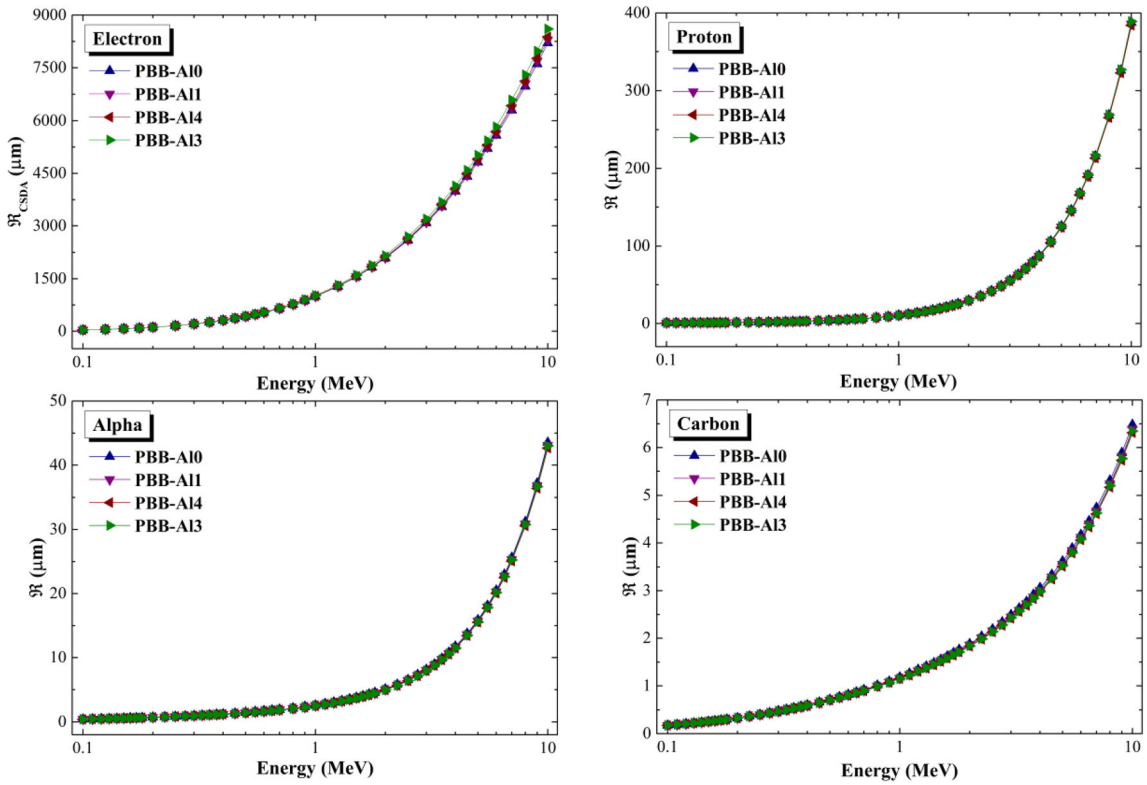

Fig. 14 Variation of range as a function of kinetic energy in the PbO–Bi_2O_3–B_2O_3–$Al(PO_3)_3$ glasses shown for electron, proton, alpha particles, and heavy carbon ion

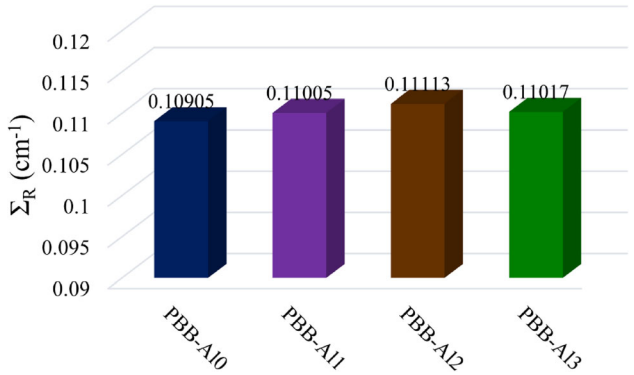

Fig. 15 Variation of removal cross-section ($\sum R$) for the novel PbO–Bi_2O_3–B_2O_3–$Al(PO_3)_3$ glasses for fast neutron

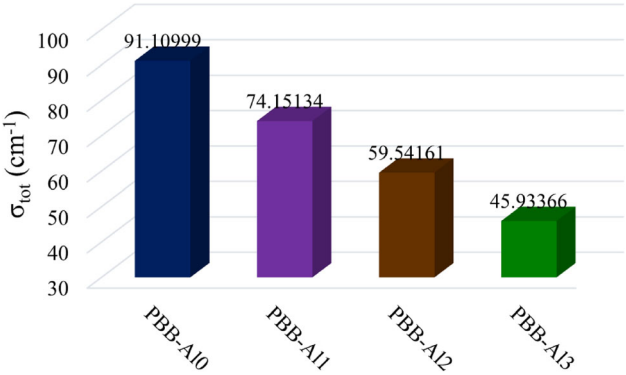

Fig. 16 Variation of total cross-section (σ_{tot}) for the novel PbO–Bi_2O_3–B_2O_3–$Al(PO_3)_3$ glasses for thermal neutron

shielding capacity of the glasses declined slightly as the concentration of $Al(PO_3)_3$ changed from 0 to 7.5 mol %. However, the influence of $Al(PO_3)_3$ on the charged particle shielding abilities of the glasses was not so significant. Furthermore, Σ_R ranged between 0.1095 and 0.11113 cm^{-1} with PBB-Al2 having the superior value. For thermal neutrons, however, the value of σ_{tot} declined as $Al(PO_3)_3$ concentration increased due to decrease in the weight fraction of B, Pb, and Bi. On the other hand, the scattering cross-section of cold neutrons in the glasses rose throughout the considered energy spectrum as $Al(PO_3)_3$ concentration declined in the glass matrix. Comparatively, the investigated PBB-Alx glasses are better photon shields than ordinary concrete, RS-360 commercial glass shield, P2 polymer, and some recently investigated glass shields. Also, the fast neutron removal ability of PBB-Al2 is better than that of

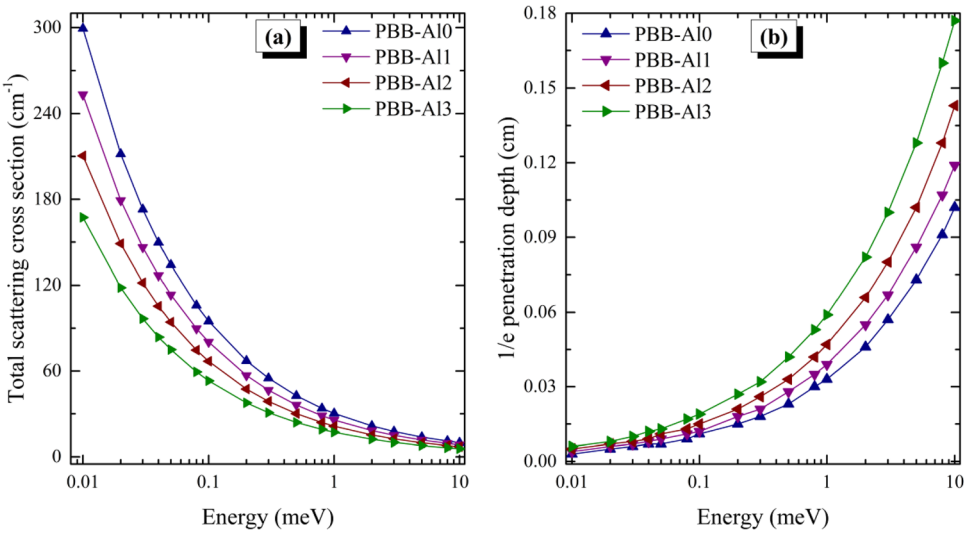

Fig. 17 Variations of **a** total cross-section of neutrons and **b** penetration depth as a function of neutron energy in the PbO–Bi_2O_3–B_2O_3–$Al(PO_3)_3$ glasses

ordinary concrete. This study reveals that the presently investigated glasses have a significant role to play as alternative radiation shields in contemporary and future application of radiation.

Acknowledgements

This research was funded by the Deanship of Scientific Research at Princess Nourah bint Abdulrahman University through the Fast-Track Path of Research Funding Program. Moreover, the authors extend their appreciation to the Deanship of Scientific Research at King Khalid University, Saudi Arabia for funding this work through Research Groups Program under grant number G.R.P1/137/42.

Funding

This study was funded by King Khalid University (G.R.P1/137/42).

References

1. J.S. Alzahrani, Z.A. Alrowaili, I.O. Olarinoye, M.A. Alothman, A.M. Al-Baradi, I. Kebaili, M.S. Al-Buriahi, Nuclear shielding properties and buildup factors of Cr-based ferroalloys. Prog. Nucl. Energy **141**, 103956 (2021)
2. G. Kilic, F. I. E. Agawany, B. O. Ilik, K. A. Mahmoud, E. Ilik, Y. S. Rammah, Ta_2O_5 reinforced Bi_2O_3–TeO_2–ZnO glasses: fabrication, physical, structural characterization, and radiation shielding efficacy. Optical Mater (2021) https://doi.org/10.1016/j.optmat.2020.110757
3. R. Kurtulus, C. Kurtulus, T. Kavas, Physical, optical, thermal, mechanical, and photon shielding properties of Rb_2O-reinforced SiO_2–Na_2O–CaO–MgO–Al_2O_3 glass system. J. Mater. Sci. Mater. Electron. **32**(6), 7801–7814 (2021). https://doi.org/10.1007/s10854-021-05500-w
4. S. Alomairy, Z. A. Alrowaili, Imen Kebaili, E. A. Wahab, C. Mutuwong, M. S. Al-Buriahi, K. S. Shaaban, Synthesis of Pb_3O_4–SiO_2–ZnO–WO_3 glasses and their fundamental properties for gamma shielding applications. Silicon 1: 1–11 (2021)
5. M.S. Al-Buriahi, M. Rashad, A. Alalawi, M.I. Sayyed, Effect of Bi_2O_3 on mechanical features and radiation shielding properties of boro-tellurite glass system. Ceram. Int. **46**(10), 16452–16458 (2020). https://doi.org/10.1016/j.ceramint.2020.03.208
6. A.S. Abouhaswa, M.H.A. Mhareb, A. Alalawi, M.S. Al-Buriahi, Physical, structural, optical, and radiation shielding properties of B_2O_3–$20Bi_2O_3$–$20Na_2O_2$–Sb_2O_3 glasses: role of Sb_2O_3. J. Non. Cryst. Solids **543**, 120130 (2020). https://doi.org/10.1016/j.jnoncrysol.2020.120130
7. K. Chandra Sekhar, N. Narsimlu, M. S. Al-Buriahi, H. A. Yakout, I. O. Olarinoye, S. Alomairy, M.D. Shareefuddin, Synthesis, optical, and radiation attenuation properties of CaF_2–TeO_2–$Na_2B_4O_7$–CuO glass system for advanced shielding applications. Eur. Phys. J. Plus 136 (9): 903 (2021)
8. R. Kurtulus, T. Kavas, I. Akkurt, K. Gunoglu, Theoretical and experimental gamma-rays attenuation characteristics of waste soda-lime glass doped with La_2O_3 and Gd_2O_3. Ceram. Int. **47**(6), 8424–8432 (2020). https://doi.org/10.1016/j.ceramint.2020.11.207

9. M.A. Alothman, M. S. Al-Buriahi, H. H. Saleh, Sultan Alomairy, B. T. Tonguç, Polarizability, metallization criterion, and radiation attenuation performance of pure and Ag-doped poly (vinyl alcohol) polymers for advanced shielding applications. J. Polym. Res. 28 (10), 1–10 (2021)
10. Y.S. Rammah, M.S. Al-Buriahi, C. Sriwunkum, M.S. Shams, E.S. Yousef, Influence of Er^{3+}-doped ions on the linear/nonlinear optical characteristics and radiation shielding features of TeO_2–ZnO–Er_2O_3 glasses. J. Mater. Sci. Mater. Electron. (2020). https://doi.org/10.1007/s10854-020-04657-0
11. J. S. Alzahrani, M. A. Alothman, Canel Eke, Hanan Al-Ghamdi, Dalal Abdulldh Aloraini, M. S. Al-Buriahi, Simulating the radiation shielding properties of TeO_2–Na_2O–TiO glass system using PHITS Monte Carlo code. Comput. Mater. Sci. 196, 110566 (2021)
12. M.S. Al-Buriahi, V.P. Singh, Comparison of shielding properties of various marble concretes using GEANT4 simulation and experimental data. J. Aust. Ceram. Soc. **56**(3), 1127–1133 (2020)
13. M. S. Al-Buriahi, T. A. Taha, Miysoon A. Alothman, Hossam Donya, I. O. Olarinoye, Influence of WO_3 incorporation on synthesis, optical, elastic and radiation shielding properties of borosilicate glass system. Eur. Phys. J. Plus 136 (7), 1–23 (2021)
14. M. A. Alothman, Z. A. Alrowaili, Sultan Alomairy, Canel Eke, C. Mutuwong, H. O. Tekin, B. T. Tonguç, M. S. Al-Buriahi, The significant role of CeO_2 content on the radiation shielding performance of Fe_2O_3–P_2O_5 glass-ceramics: geant4 simulations study. Phys. Scr. 96 (11), 115305 (2021)
15. M. S. Al-Buriahi, I. O. Olarinoye, Sultan Alomairy, Imen Kebaili, Rumeysa Kaya, Halil Arslan, Baris T. Tonguc, Dense and environment friendly bismuth barium telluroborate glasses for nuclear protection applications. Prog. Nucl. Energy 137, 103763 (2021)
16. T. Kavas, R. Kurtulus, K.A. Mahmoud, M.I. Sayyed, I. Akkurt, K. Gunoglu, Radiation shielding competencies for waste soda–lime–silicate glass reinforced with Ta_2O_5: experimental, computational, and simulation studies. Appl. Phys. A Mater. Sci. Process **127**(164), 1–14 (2021). https://doi.org/10.1007/s00339-021-04323-0
17. Y. S. Rammah, M. S. Al-Buriahi, A. S. Abouhaswa, B_2O_3–$BaCO_3$–Li_2O_3 glass system doped with Co_3O_4: structure, optical, and radiation shielding properties. Phys. B Condens. Matter. 576, 411717 (2020) https://doi.org/10.1016/j.physb.2019.411717
18. R. Kurtulus, T. Kavas, K.A. Mahmoud, I. Akkurt, K. Gunoglu, M.I. Sayyed, The effect of Nb_2O_5 on waste soda-lime glass in gamma-rays shielding applications. J. Mater. Sci. Mater. Electron. **32**(4), 4903–4915 (2021). https://doi.org/10.1007/s10854-020-05230-5
19. K. Chandra Sekhar, Abdul Hameed, N. Narsimlu, Jamila S. Alzahrani, Miysoon A. Alothman, I. O. Olarinoye, M. S. Al-Buriahi, Md Shareefuddin, Synthesis, optical, structural, and radiation transmission properties of PbO/Bi_2O_3/B_2O_3/Fe_2O_3 glasses: an experimental and in silico study. Optical Mater. 117, 111173 (2021)
20. J. S. Alzahrani, Z. A. Alrowaili, H. H. Saleh, Ateyyah M. Al-Baradi, Miysoon A. Alothman, M. S. Al-Buriahi, A significant role of Tb_2O_3 on the optical properties and radiation shielding performance of Ga_2O_3–B_2O_3–Al_2O_3–GeO_2 glasses. J. Inorg. Organomet. Polym. Mater. 1–13 (2021)
21. Wahab, EA Abdel, Kh S. Shaaban, Sultan Alomairy, M. S. Al-Buriahi, Electronegativity and optical basicity of glasses containing Na/Pb/B and their high performance for radiation applications: role of ZrO_2 nanoparticles. Eur. Phys. J. Plus 136 (6), 1–30 (2021)
22. R. Kurtulus, T. Kavas, The role of B_2O_3 in lithium-zinc-calcium-silicate glass for improving the radiation shielding competencies. J. Boron **6**(1), 236–242 (2021). https://doi.org/10.30728/boron.841726
23. I. O. Olarinoye, Sultan Alomairy, Chahkrit Sriwunkum, H. H. Hegazy, M. S. Al-Buriahi, Effects of TeO_2 and B_2O_3 on photon, neutron, and charged particle transmission properties of Bi_2O_3–BaO–LiF glass system. J. Aus. Ceram. Soc. 1–12 (2021)
24. M. A. Alothman, Z. A. Alrowaili, Jamila S. Alzahrani, EA Abdel Wahab, I. O. Olarinoye, Chahkrit Sriwunkum, Kh S. Shaaban, M. S. Al-Buriahi, Significant influence of MoO_3 content on synthesis, mechanical, and radiation shielding properties of B_2O_3–$Pb3O_4$–Al_2O_3 glasses. J. Alloys Compd. 160625 (2021)
25. K.A. Naseer, K. Marimuthu, M.S. Al-Buriahi, A. Alalawi, H.O. Tekin, Influence of Bi_2O_3 concentration on barium-telluro-borate glasses: physical, structural and radiation-shielding properties. Ceram. Int. **47**(1), 329–340 (2021). https://doi.org/10.1016/j.ceramint.2020.08.138
26. B. T. Tonguc, Halil Arslan, Mohammed Sultan Al-Buriahi, Studies on mass attenuation coefficients, effective atomic numbers and electron densities for some biomolecules, Radiat. Phys. Chem. 153, 86–91 (2018)
27. F.R. Arthur, L.J. Cox, R.F. Barrett, T.E. Booth, J.F. Briesmeister, F.B. Brown et al., MCNP^{TM} version 5. Nucl. Instrum. Methods Phys. Res. Sect. B **213**, 82–86 (2004)
28. S. Agostinelli, J. Allison, K. Amako, J. Apostolakis, H. Araujo et al., GEANT4 - a simulation toolkit. Nucl. Instrum. Methods Phys. Res. Sect. B **506**, 250–303 (2003)
29. S. Tatsuhiko, N. Koji, M. Norihiro, H. Shintaro, I. Yosuke, N. Shusaku, O. Tatsuhiko, I. Hiroshi, N. Hiroshi, F. Tokio, O.

Keisuke, K. Tetsuya, C. Satoshi, F. Takuya, S. Lembit, Particle and heavy ion transport code system, PHITS, version 2.52. J. Nucl. Sci. Technol. **50**, 913–923 (2013)
30. H. Hirayama, Y. Namito, F.B. Alex, J.W. Scott, R.N. Walter, *The EGS5 Code System* (Stanford University, Stanford Linear Accelerator Center, Stanford, California, 2005)
31. F. Salvat, J. M. Fernández-Varea, E. Acosta, J. Sempau (2001) Penelope - a code system for Monte Carlo simulation of electron and photon transport. Nuclear Energy Agency, Organisation for Economic Co-operation and Development, Barcelona, Spain.
32. A. Ferrari, P.R. Sala, A. Fasso, R. Johannes, *FLUKA: A Multi-Particle Transport Code* (Stanford University, Stanford Linear Accelerator Center, Stanford, California, 2005)
33. Imed Boukhris, Imen Kebaili, M. S. Al-Buriahi, Amani Alalawi, A. S. Abouhaswa, Barıs Tonguc, Photon and electron attenuation parameters of phosphate and borate bioactive glasses by using Geant4 simulations. Ceram. Int. 46 (15), 24435–24442 (2020)
34. M. S. Al-Buriahi, D. K. Gaikwad, H. H. Hegazy, C. Sriwunkum, R. Neffati, Fe-based alloys and their shielding properties against directly and indirectly ionizing radiation by using FLUKA simulations. Phys. Script. 96(4), 045303 (2021)
35. M. S. Al-Buriahi, Esraa M. Bakhsh, Barıs Tonguc, Sher Bahadar Khan. Mechanical and radiation shielding properties of tellurite glasses doped with ZnO and NiO. Ceram. Int. 46 (11), 19078–19083 (2020)
36. M.S. Al-Buriahi, B. Tonguç, U. Perişanoğlu, E. Kavaz, The impact of Gd_2O_3 on nuclear safety proficiencies of TeO_2–ZnO–Nb_2O_5 glasses: a GEANT4 Monte Carlo study. Ceram. Int. **46**(15), 23347–23356 (2020)
37. M. S. Al-Buriahi, V. P. Singh, Amani Alalawi, Chahkrit Sriwunkum, Baris Tamer Tonguc, Mechanical features and radiation shielding properties of TeO_2–Ag_2O–WO_3 glasses. Ceram. Int. 46 (10), 15464–15472 (2020)
38. H. An, P. Qian, Y. Ye, S. Wang, Structural and magneto-optical properties of PbO–Bi_2O_3–B_2O_3–$Al(PO_3)_3$ glasses. J. Non. Cryst. Solids **538**, 120021 (2020). https://doi.org/10.1016/j.jnoncrysol.2020.120021
39. I. Olarinoye, Variation of effective atomic numbers of some thermoluminescence and phantom materials with photon energies. Res. J. Chem. Sci. **1**(2), 64–69 (2011)
40. S.R. Manohara, S.M. Hanagodimath, K.S. Thind, Leif Gerward, On the effective atomic number and electron density: a comprehensive set of formulas for all types of materials and energies above 1 keV, Nucl. Instrum. Methods Phys. Res. Sect. B Beam Interact. Mater. Atoms 266 (18), 3906–3912 (2008)
41. Y.S. Rammah, I.O. Olarinoye, F.I. El-Agawany, A. El-Adawy, Environment friendly La^{3+} ions doped phosphate glasses/-glass-ceramics for gamma radiation shielding: their potential in nuclear safety applications. Ceram. Int. **46**(17), 27616–27626 (2020). https://doi.org/10.1016/j.ceramint.2020.07.256
42. M. S. Al-Buriahi, C. Sriwunkum, Halil Arslan, Baris T. Tonguc, Mohamed A. Bourham, Investigation of barium borate glasses for radiation shielding applications. Appl. Phys. A 126 (1), 1–9 (2020)
43. J.F. Ziegler, M.D. Ziegler, J.P. Biersack, SRIM - the stopping and range of ions in matter (2010). Nucl. Instrum. Methods B **268**, 1818–1823 (2010)
44. M. J. Berger, J. S. Coursey, M. A. Zucker, ESTAR, PSTAR, and ASTAR: computer programs for calculating stopping-power and range tables for electrons, protons, and helium ions (version 1.21) 1999.
45. I. O. Olarinoye, F. I. El-Agawany, A. El-Adawy, Y. S. Rammah. Mechanical features, alpha particles, photon, proton, and neutron interaction parameters of TeO_2–V_2O_3–MoO_3 semiconductor glasses. https://doi.org/10.1016/j.ceramint.2020.06.093
46. A. El-Khayatt, Calculation of fast neutron removal cross-sections for some compounds and materials. Ann. Nucl. Energy **37**(2), 218–222 (2010)
47. R. Kurtulus, T. Kavas, K.A. Mahmoud, I. Akkurt, K. Gunoglu, M.I. Sayyed, Evaluation of gamma-rays attenuation competences for waste soda-lime glass containing MoO_3: experimental study, XCOM computations, and MCNP-5 results. J. Non. Cryst. Solids **557**, 120572 (2021). https://doi.org/10.1016/j.jnoncrysol.2020.120572
48. S. Stalin et al., Influence of Bi_2O_3/WO_3 substitution on the optical, mechanical, chemical durability and gamma ray shielding properties of lithium-borate glasses. Ceram. Int. **47**(4), 5286–5299 (2021). https://doi.org/10.1016/j.ceramint.2020.10.109
49. I. I. Bashter, Calculation of radiation attenuation coefficients for shielding concretes. Ann. Nucl. Energy. 24(17), 1389–1401 (1997) https://doi.org/10.1016/S0306-4549(97)00003-0
50. A.G. Schott, http://www.schott.com/advancedoptics/English/products/opticalmate-rials/specialmaterials/radiation-shielding-glasses/index.html.
51. M. S. Al-Buriahi, et al., Radiation attenuation properties of some commercial polymers for advanced shielding applications. Polym. Adv. Technol. 1–11 (2021) https://doi.org/10.1002/pat.5267
52. H. H. Hegazy, et al., Nuclear shielding properties of B_2O_3–Bi_2O_3–SrO glasses modified with Nd_2O_3: theoretical and

simulation studies. Ceram. Int. 47(2) 2772–2780 (2021) https://doi.org/10.1016/j.ceramint.2020.09.131

53. Y.S. Rammah et al., Investigations on borate glasses within SBC-Bx system for gamma-ray shielding applications. Nucl. Eng. Technol. **53**(1), 282–293 (2021). https://doi.org/10.1016/j.net.2020.06.034
54. M. S. Al-Buriahi, et al., Newly developed glasses containing Si/Cd/Li/Gd and their high performance for radiation applications: role of Er_2O_3. J. Mater. Sci.: Mater. Electron. (2021) https://doi.org/10.1007/s10854-021-05608-z
55. I.O. Olarinoye, Y.S. Rammah, S. Alraddadi, C. Sriwunkum, A.F. Abd El-Rehim, H.Y. Zahran, M.S. Al-Buriahi, The effects of La_2O_3 addition on mechanical and nuclear shielding properties for zinc borate glasses using Monte Carlo simulation. Ceram. Int. **46**(18), 29191–29198 (2020). https://doi.org/10.1016/j.ceramint.2020.08.092